Research Article | Vol. 12, No. 1 / 1 Jan 2022 / Optical Materials Express 308
Optical Materials EXPRESS

Rubidium copper chloride scintillator for X-ray imaging screen

WORAKIT NAEWTHONG,[1,5] WARIDSARAPORN JUNTAPO,[1] RATTHASART AMARIT,[1] KAMONCHANOK DUANGKANYA,[1] SARUN SUMRIDDETCHKAJORN,[2] THITI RUNGSEESUMRAN,[3] NATTHAPORN KAMWANG,[3] YAOWALUK TARIWONG,[4] JAKRAPONG KAEWKHAO,[4] AND ATCHA KOPWITTHAYA[1,5,*]

[1]*Photonics Technology Research Team, National Electronics and Computer Technology Center, Pathum Thani 12120, Thailand*
[2]*National Electronics and Computer Technology Center, Pathum Thani 12120, Thailand*
[3]*Thailand Institute of Nuclear Technology (Public Organization), Nakorn Nayok 26120, Thailand*
[4]*Center of Excellence in Glass Technology and Materials Science (CEGM), Nakhon Pathom Rajabhat University, Nakhon Pathom, 73000, Thailand*
[5]*These authors are equally contributed*
[*]*atcha.kopwitthaya@nectec.or.th*

Abstract: Metal halide-based perovskite materials have received great attention in scintillating applications because they can emit strong visible light when interacting with X-ray particles. Here, we report a scintillator based on rubidium copper chlorine incorporated in the polydimethylsiloxane matrix. The scintillator shows a bright violet emission under ultraviolet and ionizing radiation. The temperature-dependent photoluminescence and radioluminescence shows maximum thermal enhancement at 80°C and 60°C, respectively. Moreover, the first X-ray image from this material reveals the detailed information of the object captured by a commercially available digital camera, indicating a potent scintillator for creating X-ray imaging screens.

1. Introduction

Scintillating materials have ability to transform ionizing radiation into visible photons. Many applications including space exploration, industrial inspection, security, and medical radiography require a high quality and good performance of X-ray scintillator [1–4]. However, conventional scintillator still undergoes limitations in terms of high-temperature manufacturing, low light yield, and toxicity concern [5,6]. Therefore, new classes of high-performance scintillator with cost effective and environmentally friendly are of interest.

Metal halide perovskite has recently received a great attention in scintillator application. To be specific, lead halide is one of the most popular materials due to high photoluminescence quantum yield, wide color gamut, and low-temperature synthesis protocol [7–11]. Although many reports have demonstrated quality X-ray images from lead halide scintillators, toxicity of lead element is a limitation for practical usages. There are many attempts to replace lead with other elements such as antimony (Sb), silver (Ag), bismuth (Bi), copper (Cu) and manganese (Mn) [12–19]. Rubidium copper halide is the emerging lead-free structure that has been recently reported to be a prospective scintillator with high light yield [20]. However, X-ray image from this structure has not been reported yet.

Here, we demonstrate our proposed facile preparation of high-performance and environmentally-friendly polydimethylsiloxane (PDMS) scintillator based on a rubidium copper halide (Rb_2CuCl_3). This proposed preparation of the scintillator shows strong violet emission and thermal enhancement

#444631 https://doi.org/10.1364/OME.444631
Journal © 2022 Received 1 Oct 2021; revised 15 Dec 2021; accepted 15 Dec 2021; published 23 Dec 2021

Optical Materials EXPRESS

behavior in both photoluminescence (PL) and radioluminescence (RL) studies. The first X-ray image acquired from a commercial digital camera with Rb_2CuCl_3 scintillator reveals a potential visualization tool for X-ray radiography.

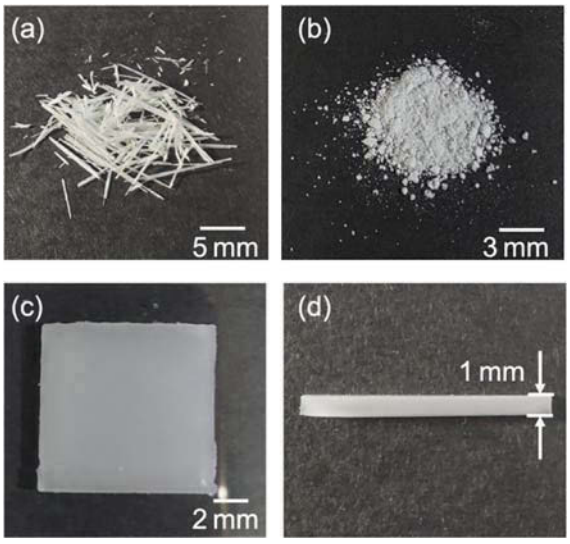

Fig. 1. a) Photograph of dried rod-like Rb_2CuCl_3 crystals. (b) Crystal powder after grinding. (c) Top-view and (d) side-view of Rb_2CuCl_3/PDMS scintillator under natural light.

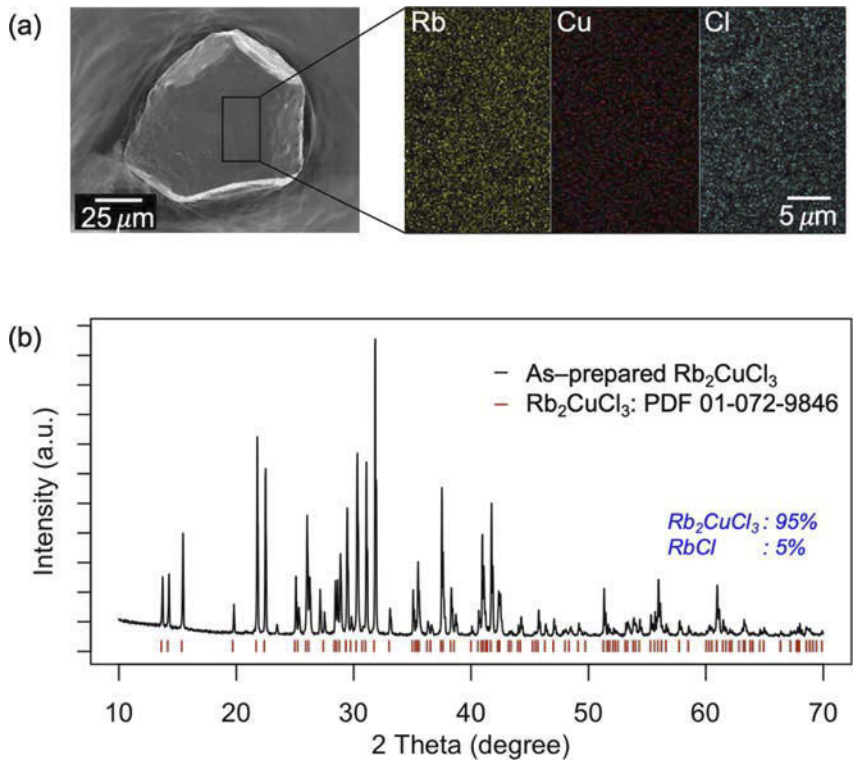

Fig. 2. (a) SEM image and the element mapping taken by EDS. (b) XRD pattern of as-prepared Rb_2CuCl_3 (black line) and standard powder diffraction profile of Rb_2CuCl_3 (red line)

Optical Materials EXPRESS

2. Experimental procedures (copper halide scintillator preparation)

Rb_2CuCl_3 was synthesized by a solution cooling method modified from Zhao's protocol [20]. The reaction was done under nitrogen atmosphere to prevent an oxidation of Cu^+ at 135°C. Then, rod-like crystals were obtained when solution was cooled down to room temperature. The crystals were purified with isopropyl alcohol for several times and dried in vacuum. Figure 1(a) shows dried rod-like Rb_2CuCl_3 crystals before grinding into powder in Fig. 1(b). After that, the Rb_2CuCl_3 powder was embedded into the PDMS matrix, so called Rb_2CuCl_3/PDMS. The uniform crystal distribution in PDMS was occurred under sonication for 30 minutes. This will help to maximize luminescence from the scintillator comparing to the non-sonication sample (Figure S1 in Supplement 1). Finally, the Rb_2CuCl_3 scintillator, as shown in Figs. 1(c,d) with dimensions of 10 mm x 10 mm x 1 mm was kept under vacuum for further uses.

3. Results and discussion

3.1. Material characterization

Morphology and elemental analysis of the crystal were analyzed with field-emission scanning electron microscope (FE-SEM SU8030) and energy-dispersive X-ray spectrometers (EDS), respectively. Figure 2(a) demonstrates an SEM image of grinding Rb_2CuCl_3 crystal with average size of 50 μm. Inside the crystal, EDS elemental mapping shows homogenous distribution of rubidium (Rb), copper (Cu) and chlorine (Cl). Moreover, quantitative analysis of EDS spectra (Figure S2 in Supplement 1) indicates atomic percentages of Rb, Cu and Cl elements as 24.05, 16.17 and 59.78%, respectively. This observed ratio is closed to stoichiometric ratio of Rb_2CuCl_3 which indicates successful formation of crystal. In addition, the crystallographic properties were characterized using X-Ray diffraction (XRD). Figure 2(b) is the graphical

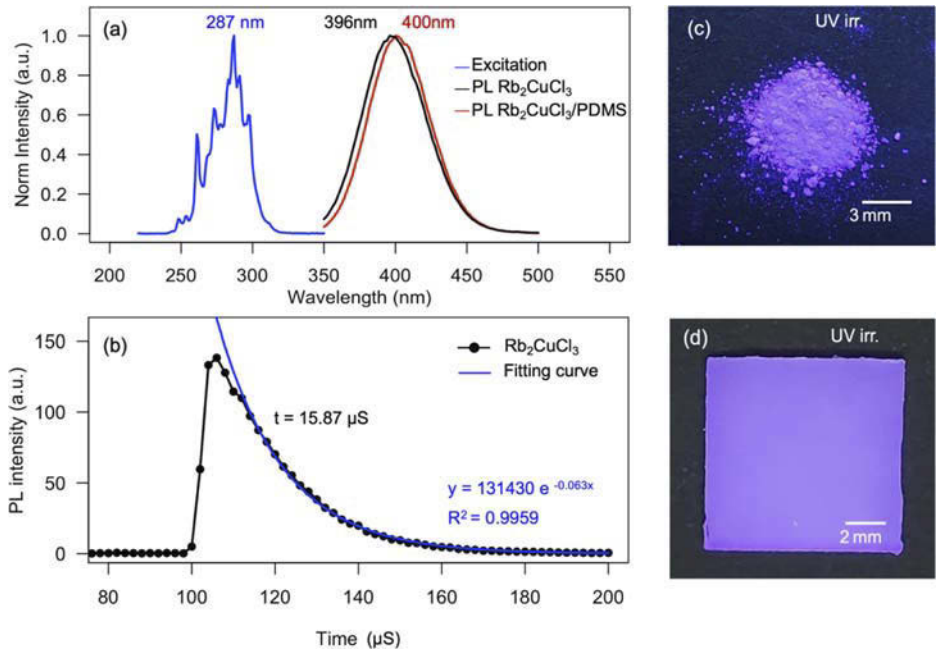

Fig. 3. (a) Photoluminescence of Rb_2CuCl_3 powder and Rb_2CuCl_3/PDMS with excitation spectrum. (b) Time-resolved PL decay spectrum with 287nm excitation. (c) Photograph of Rb_2CuCl_3 powder and (d) Rb_2CuCl_3/PDMS under UV irradiation.

Optical Materials EXPRESS

result of Rietveld refinement of XRD pattern acquired from as-prepared Rb_2CuCl_3 powder, revealing an orthorhombic crystal structure of Rb_2CuCl_3(Pnma) with unit cell parameters of a =12.501 Å, b = 4.272 Å, c = 13.000 Å. It is in a good agreement with the previous report, then the PLQY of this structure should be around 99% [20]. Additionally, small amount of RbCl precursor (5%) was found in the product. It is worth noting that the leftover reactant may cause hygroscopic phenomena leading to degradation under ambient conditions [21]. However, the Rb_2CuCl_3/PDMS is tolerant to ambient atmosphere for a short period of time, i.e., 72 hours. To prolong a stability, moistureless storage is required to retard a degradation.

3.2. Optical response of the Rb_2CuCl_3 scintillator

The photoluminescence (PL) of sample and excitation wavelength are shown in Fig. 3(a). With the same excitation at a 287 nm ultraviolet (UV) wavelength, Rb_2CuCl_3 powder exhibits emission peak at 396 nm with full-width-at-half-maximum (FWHM) of 50 nm whereas Rb_2CuCl_3/PDMS shows 400 nm peak with a FWHM of 48 nm. A slightly red-shifted peak may attribute to PDMS incorporation. It is clearly seen that the scintillator has a large stoke shift and negligible excitation overlap, referring to be a potentially self-absorption-free scintillator. The PL decay spectrum was recorded under 287 nm excitation at room temperature. The exponential fitting indicates the decay lifetime at 15.87 μs as shown in Fig. 3(b). In addition, Figs. 3(c) and 3(d) present a bright violet emission from both powder and Rb_2CuCl_3/PDMS under 254 nm wavelength UV

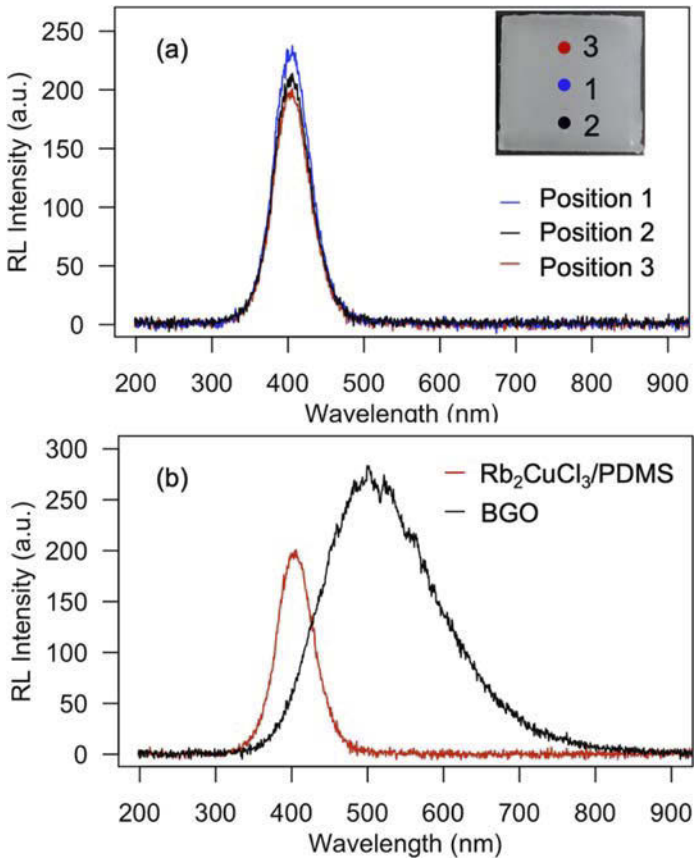

Fig. 4. (a) Spatial uniformity of Rb_2CuCl_3/PDMS scintillator and (b) rdRadioluminescence of Rb_2CuCl_3/PDMS comparing to commercially available BGO scintillator.

Optical Materials EXPRESS

lamp. Although the quantum efficiency of conventional CCD and CMOS is high in green region, the broadband detector can also be found in the market. However, shifted in emission is still of interest for future study and may be done by doping other materials to change the intrinsic properties of materials [9,22].

3.3. Spatial uniformity and temperature-dependent behavior

To study the spatial uniformity, RL at different positions of scintillator was recorded. As shown in Fig. 4(a), there are slightly differences in emission intensity of each position. In an attempt to compare RL light yield with the commercial product, a bismuth germanate scintillator crystal (BGO) was used as a reference standard (Fig. 4(b)). Additionally, the temperature-dependent PL measurement of Rb_2CuCl_3/PDMS was investigated between room temperature to 90 °C. The PL intensity was gradually increased and reached a maximum intensity at 80 °C when temperature was elevated. The enhancement can be described by thermoluminescence (TL) of photon trapping and recombining of materials [23]. Then, PL began to drop beyond this point as shown in Fig. 5(a). This result is in a good agreement of the thermal quenching at high temperature, i.e., above 373K [20]. Moreover, the robust emission of scintillator can be regenerated after cooling down. The temperature-dependent of RL was also studied here, and we found that the scintillator underwent the thermal enhancement followed by quenching. The intensity drop occurred in 60 °C which is lower than that of UV excitation as shown in Fig. 5(b). Moreover, RL response has 7 nm-red-shifted comparing to PL emission peak, but no different in terms of FWHM (Figure S3 in Supplement 1).

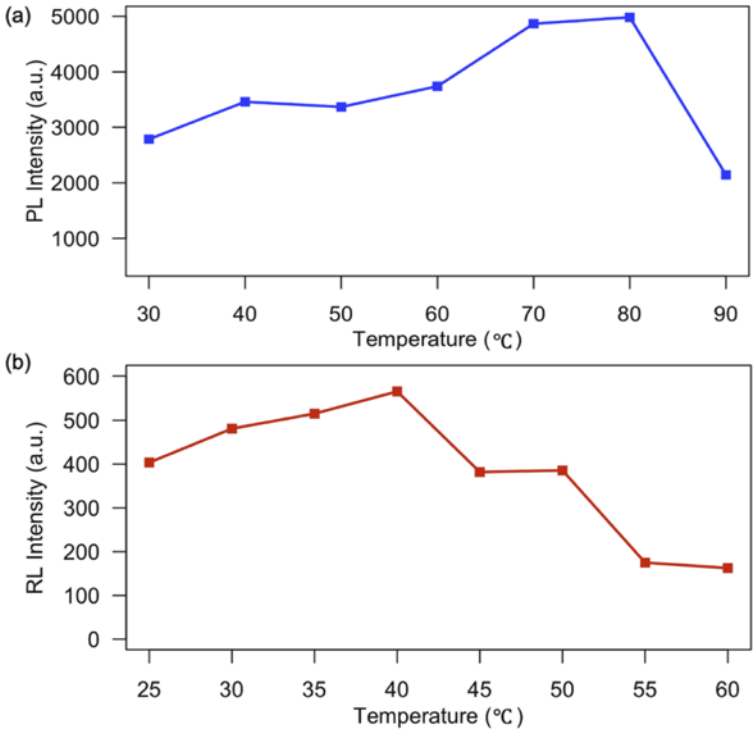

Fig. 5. (a) Temperature-dependent photoluminescence and (b) Radioluminescence of Rb_2CuCl_3/PDMS.

Optical Materials EXPRESS

3.4. X-ray study and imaging

In Fig. 6(a), the X-ray absorption coefficient was investigated in ranges of 10 to 60 keV with Amptek detector, model: XR-100T-CdTe, with a current of 200 μA at exposure time of 300 seconds. The absorption of Rb_2CuCl_3/PDMS scintillator is still lower than that of the reference standard, Dupont Cronex DETA II UG 002814, due to low density of scintillator material embedded in PDMS. It may be a future work to develop a process of high-density packing in plastic or polymer scintillator to overcome this issue. Moreover, response of Rb_2CuCl_3/PDMS scintillator was further studied by applying a working voltage at 60 kV and current of 10 to 40 mA. The emission intensity from the scintillator was captured using a digital camera and average pixel values were calculated from the region of interest (ROI) of 400×400 pixels. The dose rate-dominated linear response of Rb_2CuCl_3/PDMS scintillator can be observed in the ranges of 100 to 350 μGy/s with well-fitting to linear function ($R^2 = 0.996$), as shown in Fig. 6(b). Additionally, the signal-to-noise variation as a function of dose rate show in Fig. 6(c). In the ranges of dose rate 80 to 300 μGy/s, the S/N is lower than 50. The S/N increases 10 times when dose rate is higher than 300 μGy/s.

To obtain an X-ray image, a piece of lead with number one shape was used as an object at 50 centimeters away from X- ray source. The X-ray beam, at working voltage of 60 kV and current of 40 mA, was pass through a 0.25 mm paper sheet before hitting an object as well as a scintillator, as shown in Fig. 7(a). The image was reflected by mirror and recorded by a commercial digital

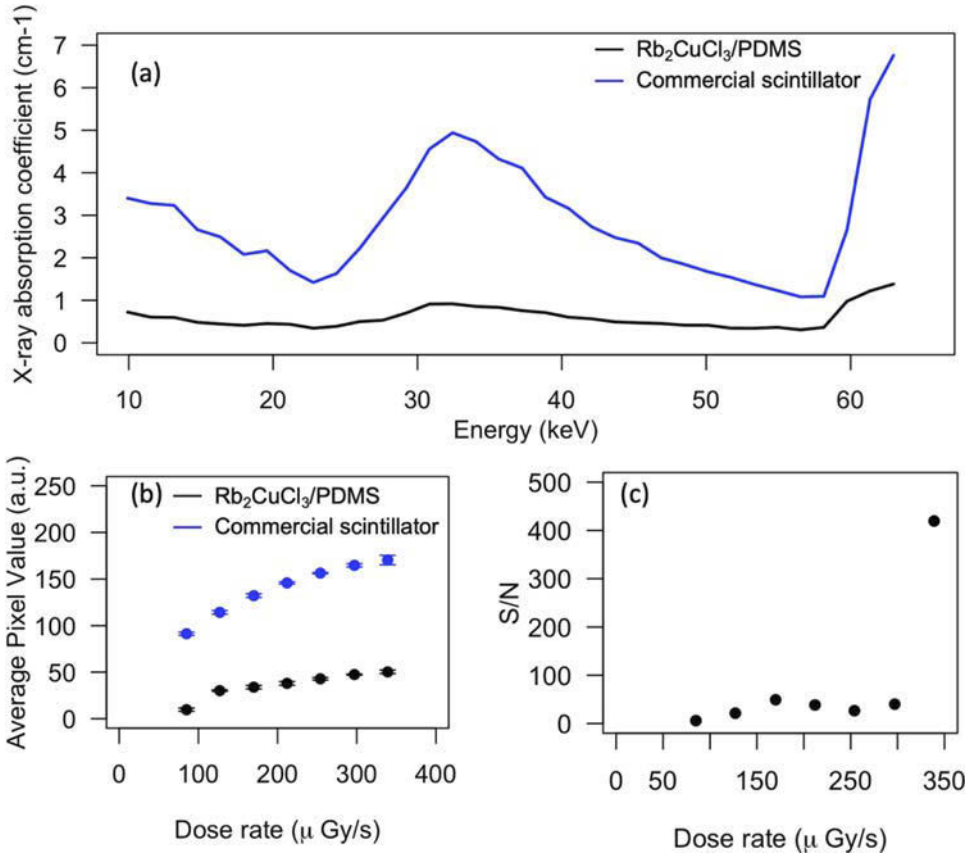

Fig. 6. (a) X-ray absorption coefficient. (b) Dose rate response. (c) Signal-to-noise variation as a function of dose rate.

Optical Materials EXPRESS

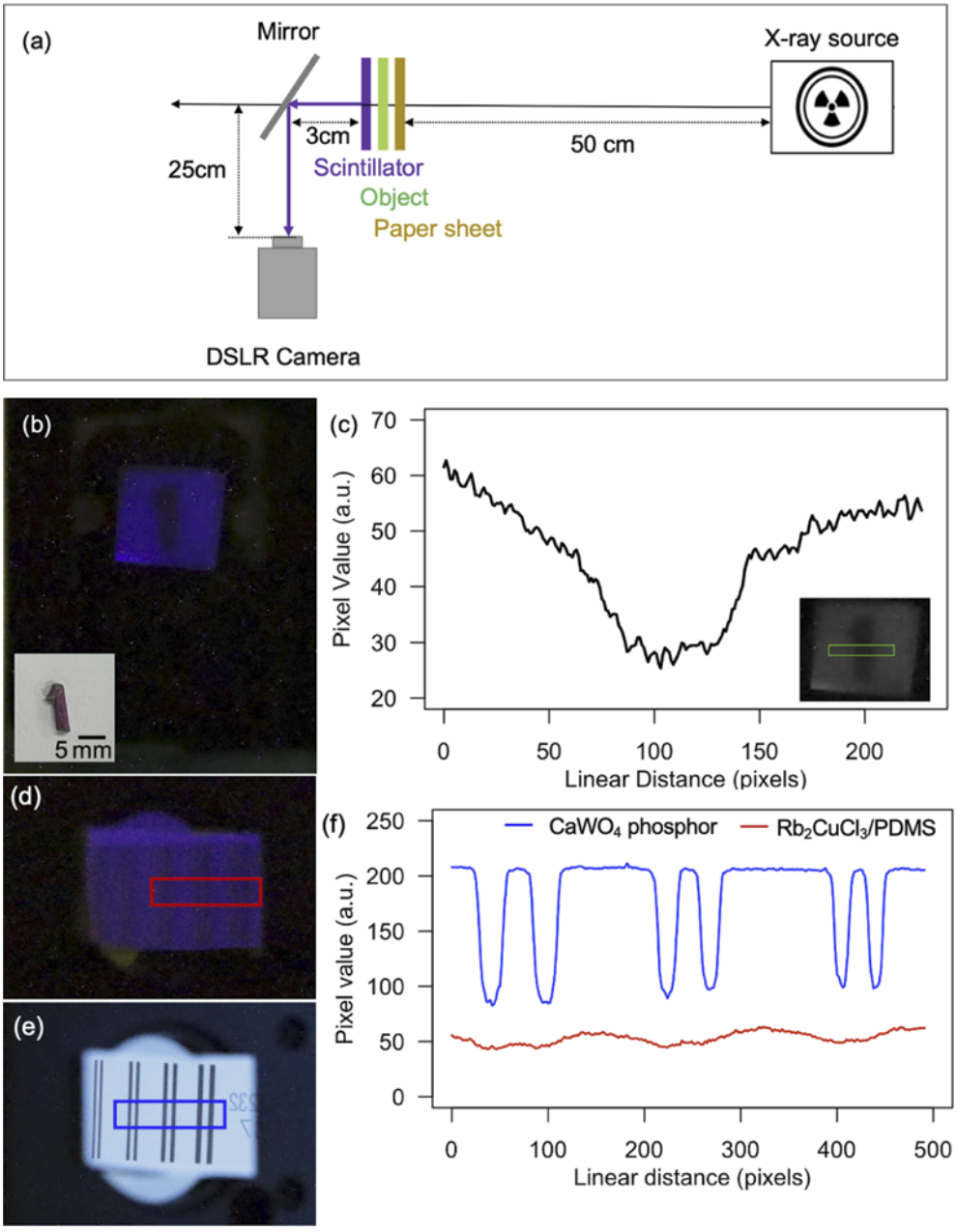

Fig. 7. (a) Schematic setup of X-ray imaging. (b) X-ray image using Rb_2CuCl_3/PDMS scintillator with exposure time at 20 seconds. The inset shows a 2 mm-thick of lead piece used as an object. (c) Intensity profile of X-ray image taken as a contrast ratio. The inset, a green rectangle, shows the region of interest (ROI). (d) X-ray image of double-wire IQI with Rb_2CuCl_3/PDMS scintillator and (e) with a commercially available $CaWO_4$ phosphor. (f) A plot of resolution obtained from (d) and (e).

camera, Canon EOS RP with EF-S18-135mm f/3.5-5.6 IS USM lens. The violet background in Fig. 7(b) illustrated emission from Rb_2CuCl_3/PDMS scintillator after exposure to X-ray beam. The intensity profile of an X-ray image shows in Fig. 7(c) with a contrast ratio of 0.349. With the

Optical Materials EXPRESS

same condition, the commercial scintillator ($CaWO_4$ phosphor, Dupont Cronex Detail) shows contrast ratio at 0.538 (Table S1). The resolution measurement was done using a double-wire IQI (Image Quality Identifier) as shown in Fig. 7(d-f). It is necessary to study the density of materials loaded in PDMS in the future work to increase the resolution. However, the first X-ray image from Rb_2CuCl_3/PDMS shows detailed information of the object. Due to a good foldability, molding ability, and high crack resistance of PDMS, the scintillator can be easily fit in any desired form with a digital camera without using grinding or polishing machine. Taking these advantages, the PDMS scintillator will provide a low manufacturing cost comparing to bulk single crystal.

4. Conclusion

In conclusion, this work has demonstrated the preparation of scintillator based on the rubidium copper chloride synthesized by cooling method. The Rb_2CuCl_3 incorporated in PDMS has a strong emission around 400 nm depending on excitation wavelengths. The thermal stability has also studied under UV and ionizing radiation. The scintillator shows thermal enhancement upon elevated temperature, then quenching is dominated at a certain temperature. Finally, the X-ray image from our scintillator discloses detailed information of an object. Our finding offers a potential scintillator with cost effective for X-ray imaging screen industry.

Funding. National Electronics and Computer Technology Center (P2051053).

Acknowledgments. The authors would like to thank Dr. Saowapak Thongvigitmanee and image team in the Assistive Technology and Medical Devices Research Center: A-MED, National Science and Technology Development Agency, for providing good comments in radiography applications. Also, the authors thank to Dr. Mati Horprathum for help identifying collaborators for this work. Also, Jakrapong Kaewkhao and Yaowaluk Tariwong would like to thanks Thailand Science Research and Innovation (TSRI) for partially supporting this research.

Disclosures. The authors declare no conflicts of interest.

Data availability. Data underlying the results presented in this paper are not publicly available at this time but may be obtained from the authors upon reasonable request.

Supplemental document. See Supplement 1 for supporting content.

References

1. A. Owens, "Scintillators on interplanetary space missions," IEEE Trans. Nucl. Sci. **55**(3), 1430–1436 (2008).
2. D. Rinaldi and L. Montalto, "Scintillator crystals: structure, characterization and models for better performances," Crystals **10**(2), 96 (2020).
3. Q. Chen, J. Wu, X. Ou, B. Huang, J. Almutlaq, A. A. Zhumekenov, X. Guan, S. Han, L. Liang, Z. Yi, J. Li, X. Xie, Y. Wang, Y. Li, D. Fan, D. B. L. Teh, A. H. All, O. F. Mohammed, O. M. Bakr, T. Wu, M. Bettinelli, H. Yang, W. Huang, and X. Liu, "All-inorganic perovskite nanocrystal scintillators," Nature **561**(7721), 88–93 (2018).
4. X. Ou, X. Qin, B. Huang, J. Zan, Q. Wu, Z. Hong, L. Xie, H. Bian, Z. Yi, X. Chen, Y. Wu, X. Song, J. Li, Q. Chen, H. Yang, and X. Liu, "High-resolution X-ray luminescence extension imaging," Nature **590**(7846), 410–415 (2021).
5. W. Chen, J. Cao, F. Hu, R. Wei, L. Chen, X. Sun, and H. Guo, "Highly efficient $Na_5Gd_9F_{32}$:Tb^{3+} glass ceramic as nanocomposite scintillator for X-ray imaging," Opt. Mater. Express **8**(1), 41–49 (2018).
6. A. Yoneyama, R. Baba, and M. Kawamoto, "Quantitative analysis of the physical properties of CsI, GAGG, LuAG, CWO, YAG, BGO, and GOS scintillators using 10-, 20- and 34-keV monochromated synchrotron radiation," Opt. Mater. Express **11**(2), 398–411 (2021).
7. M. Liu, A. Matuhina, H. Zhang, and P. Vivo, "Advances in the stability of halide perovskite nanocrystals," Materials **12**(22), 3733 (2019).
8. Y. Zhang, R. Sun, X. Ou, K. Fu, Q. Chen, Y. Ding, L.-J. Xu, L. Liu, Y. Han, A. V. Malko, X. Liu, H. Yang, O. M. Bakr, H. Liu, and O. F. Mohammed, "Metal halide perovskite nanosheet for x-ray high-resolution scintillation imaging screens," ACS Nano **13**(2), 2520–2525 (2019).
9. L. Protesescu, S. Yakunin, M. I. Bodnarchuk, F. Krieg, R. Caputo, C. H. Hendon, R. X. Yang, A. Walsh, and M. V. Kovalenko, "Nanocrystals of cesium lead halide perovskites ($CsPbX_3$, X = Cl, Br, and I): novel optoelectronic materials showing bright emission with wide color gamut," Nano Lett. **15**(6), 3692–3696 (2015).
10. J. Li, C. Ren, X. Qiu, X. Lin, R. Chen, C. Yin, and T. He, "Ultrafast optical nonlinearity of blue-emitting perovskite nanocrystals," Photonics Res. **6**(6), 554–559 (2018).
11. V. B. Mykhaylyk, H. Krausb, and M. Saliba, "Bright and fast scintillation of organolead perovskite $MAPbBr_3$ at low temperatures," Mater. Horiz. **6**(8), 1740–1747 (2019).
12. W. Zhu, W. Ma, Y. Su, Z. Chen, X. Chen, Y. Ma, L. Bai, W. Xiao, T. Liu, H. Zhu, X. Liu, H. Liu, X. Liu, and Y. Yang, "Low-dose real-time X-ray imaging with nontoxic double perovskite scintillators," Light Sci. Appl. **9**(1), 112 (2020).

Optical Materials EXPRESS

13. G. Zhou, B. Su, J. Huang, Q. Zhang, and Z. Xia, "Broad-band emission in metal halide perovskites: Mechanism, materials, and applications," Mater. Sci. Eng. R Rep. **141**, 100548 (2020).
14. V. K. Ravi, N. Singhal, and A. Nag, "Initiation and future prospects of colloidal metal halide double-perovskite nanocrystals: Cs_2AgBiX_6 (X = Cl, Br, I)," J. Mater. Chem. A **6**(44), 21666–21675 (2018).
15. J. Zhou, X. Yun, R. Wang, D. Xu, and X. Li, "Self-trapped exciton to dopant energy transfer in Sb^{3+}-doped Cs_2ZrCl_6 perovskite variants," Mater. Chem. Front. **5**(16), 6133–6138 (2021).
16. P. Sebastia-Luna, J. Navarro-Alapont, M. Sessolo, F. Palazon, and H. J. Bolink, "Solvent-free synthesis and thin-film deposition of cesium copper halides with bright blue photoluminescence," Chem. Mater. **31**(24), 10205–10210 (2019).
17. L. Xie, B. Chen, F. Zhang, Z. Zhao, X. Wang, L. Shi, Y. Liu, L. Huang, R. Liu, B. Zou, and Y. Wang, "Highly luminescent and stable lead-free cesium copper halide perovskite powders for UV-pumped phosphor-converted light-emitting diodes," Photonics Res. **8**(6), 768–775 (2020).
18. L.-J. Xu, X. Lin, Q. He, M. Worku, and B. Ma, "Highly efficient eco-friendly X-ray scintillators based on an organic manganese halide," Nat. Commun. **11**(1), 4329 (2020).
19. T. Jiang, W. Ma, H. Zhang, Y. Tian, G. Lin, W. Xiao, X. Yu, J. Qiu, X. Xu, Y. M. Yang, and D. Ju, "Highly efficient and tunable emission of lead-free manganese halides toward white light-emitting diode and x-ray scintillation applications," Adv. Funct. Mater. **31**(14), 2009973 (2021).
20. X. Zhao, G. Niu, J. Zhu, B. Yang, J.-H. Yuan, S. Li, W. Gao, Q. Hu, L. Yin, K.-H. Xue, E. Lifshitz, X. Miao, and J. Tang, "All-Inorganic copper halide as a stable and self-absorption-free x-ray scintillator," J. Phys. Chem. Lett. **11**(5), 1873–1880 (2020).
21. P. Vashishtha, D. Giovanni, M. Klein, T. C. Sum, S. G. Mhaisalkar, N. Mathews, and T. White, "Room temperature synthesis of low-dimensional rubidium copper halide colloidal nanocrystals with near unity photoluminescence quantum yield," Nanoscale **13**(1), 59–65 (2021).
22. G. Zuo, A. Xie, J. Li, T. Su, X. Pan, and W. Dong, "Large emission red-shift of carbon dots by fluorine doping and their applications for red cell imaging and sensitive intracellular ag+ detection," J. Phys. Chem. C **121**(47), 26558–26565 (2017).
23. Y. Horowitz, R. Chen, L. Oster, and I. Eliyahu, "Thermoluminescence theory and analysis: advances and impact on applications," *Encyclopedia of Spectroscopy and Spectrometry* (3rd Edition) (Academic Press, 2017), pp. 444–451.